Heat Transfer Engineering

ISSN: (Print) (Online) Journal homepage: www.tandfonline.com/journals/uhte20

Laminar Natural Convection of Water-Based Alumina Nanofluids in a Square Enclosure

Sean P. Malkeson & Nilanjan Chakraborty

To cite this article: Sean P. Malkeson & Nilanjan Chakraborty (2024) Laminar Natural Convection of Water-Based Alumina Nanofluids in a Square Enclosure, Heat Transfer Engineering, 45:14, 1173-1189, DOI: 10.1080/01457632.2023.2249727

To link to this article: https://doi.org/10.1080/01457632.2023.2249727

Published online: 03 Sep 2023.

HEAT TRANSFER ENGINEERING
2024, VOL. 45, NO. 14, 1173–1189
https://doi.org/10.1080/01457632.2023.2249727

Taylor & Francis
Taylor & Francis Group

Laminar Natural Convection of Water-Based Alumina Nanofluids in a Square Enclosure

Sean P. Malkeson[a] and Nilanjan Chakraborty[b]

[a]School of Engineering, Liverpool John Moores University, Liverpool, UK; [b]School of Engineering, Newcastle University, Newcastle upon Tyne, UK

ABSTRACT

Steady-state, laminar, natural convection of water-based alumina nanofluids in a square enclosure with partial heating from the bottom and symmetrical cooling from the sides has been investigated based on numerical simulations. The effects of Rayleigh number, normalized heat source length and nanoparticle volume fraction on the heat transfer behavior have been investigated. An increase in Rayleigh number, for given values of normalized heat source length and nanoparticle volume fraction, leads to an increase in Nusselt number. For a given set of values of Rayleigh number based on base-fluid properties and normalized heat source length, the Nusselt number does not vary significantly with increasing nanoparticle volume fraction because the strengthening viscous effects with increasing volume fraction for water-based alumina nanofluids counteracts the enhanced thermal diffusion in nanofluids. However, when effective Rayleigh number is based on nanofluid properties, Nusselt number decreases with increasing nanoparticle volume fraction. For a given set of values of Rayleigh number and nanoparticle volume fraction, the Nusselt number increases with increasing normalized heat source length due to the strengthening of advective transport. A correlation for mean Nusselt number is proposed which adequately captures qualitative and quantitative behavior obtained from the simulations across the considered parameter range.

Introduction

Natural convection in enclosed spaces has applications ranging from nuclear power stations to the preservation of canned food as well as in the cooling of electronic components. Therefore, the fundamental understanding of momentum and thermal transport across these applications is not only of academic interest but, also, of practical importance. Currently, the majority of analyses of natural convection in enclosed spaces have been conducted for two configurations. The first of these typical configurations includes differentially heated vertical sidewalls, for which the momentum and thermal transfer have been extensively analyzed for both Newtonian [1–3] and non-Newtonian [4–6] fluids. The second of these typical configurations involves differentially heated horizontal walls where the bottom wall is heated (i.e., Rayleigh-Bérnard Convection). Despite superficial similarities, the natural convection that occurs in these two configurations exhibit fundamental differences. For example, for the differentially heated vertical wall configuration the convection is established when a finite temperature difference is created between the active walls, whereas a critical Rayleigh number needs to be surpassed for the onset of convection in Rayleigh-Bérnard convection. It should be noted that the momentum and thermal transport characteristics of Rayleigh-Bérnard Convection have been analyzed in detail in previous studies for Newtonian [7, 8] and non-Newtonian [9, 10] fluids. In the majority of the previously discussed literature, only the natural convection in enclosures with differentially heated horizontal/-vertical walls were considered. However, the analysis of enclosures with locally heated walls, which are representative of the cooling of electronic components [11], is of significant importance. Aydin and Yang [11] considered the natural convection of air in a square enclosure with localized heating from below with symmetrical cooling from vertical sidewalls where the effects of Rayleigh number and non-dimensional heat source

CONTACT Dr. Sean P. Malkeson, Programme Leader s.p.malkeson@ljmu.ac.uk Mechanical Engineering, School of Engineering, Liverpool John Moores University, James Parsons Building, Byrom Street, Liverpool, L3 3AF, UK.

NOMENCLATURE

c_p	Specific heat capacity at constant pressure, J/(kg·K)
c^*	Model parameter
d	Diameter, m
f	Function
g	Acceleration due to gravity, m/s^2
h	Heat transfer coefficient, W/(m^2·K)
k	Thermal conductivity, W/(m·K)
ℓ	Length of the heat source, m
L	Length of the enclosure side, m
max	Maximum value
Nu	Nusselt number
$\overline{Nu}$	Mean Nusselt number
p	Pressure, Pa
Pr	Prandtl number
q	Heat flux, W/m^2
R^2	Coefficient of determination
Ra	Rayleigh number
Re	Reynolds number
T	Temperature, K
u_{bm}	Brownian motion velocity of nanoparticles, m/s
u_i	i^{th} component of velocity, m/s
U	Velocity, m/s
U_2	Dimensionless vertical velocity (u_2L/α)
V	Characteristic velocity in vertical direction, m/s
x_i	i^{th} component of the coordinate, m

Greek Symbols

α	Thermal diffusivity, m^2/s
β	Thermal expansion coefficient, 1/K
δ	Hydrodynamic boundary layer thickness, m
δ_{th}	Thermal boundary layer thickness, m
δ_{ij}	Kronecker delta
ρ	Density, kg/m^3
μ	Dynamic viscosity, kg/(m·s)
ν	Kinematic viscosity, m^2/s
φ	Nanoparticle volume fraction
θ	Non-dimensional temperature
τ_{ij}	Stress tensor, kg/(m·s^2)
ΔT	Temperature difference between the hot and cold walls, K

Subscripts

C	Subscript indicating cold wall
eff	Subscript indicating effective values
f	Subscript indicating base fluid property values
H	Subscript indicating hot wall
nf	Subscript indicating the nanofluid values
ref	Subscript indicating reference value
s	Subscript indicating nanoparticle property values
wf	Subscript indicating condition of fluid contacting wall

length parameters on the mean Nusselt number were investigated. It was found that the mean Nusselt number increases with increasing Rayleigh number and length of the heat source, and that the symmetrical cooling from the vertical sidewalls of the enclosure is necessary for the efficient cooling of electronic chips [11]. It should be noted, however, that the study by Aydin and Yang [11] was limited to considering Newtonian fluids (e.g., air). In many of the previous studies of this configuration [11–15], the working fluids considered were Newtonian (e.g., air and water) which have a low thermal conductivity and, therefore, do not offer high heat flux. From the perspective of enhancing heat transfer efficiencies for electronic cooling applications, non-Newtonian fluids have been considered where, typically, shear-thinning fluids are expected to offer improved heat transfer performance due to the fact that their viscosities decrease with increasing shear rates. It should further be noted that the currently considered configuration has been also investigated for yield stress fluids (i.e., materials flow only when a critical stress value known as yield stress is surpassed) by Hassan et al. [16] due to its wide range of applications in food processing. Alternatively, nanofluids (i.e., fluids containing a small quantity of nano-sized particles which are uniformly and stably suspended) offer higher thermal conductivities than that of the base fluid and, therefore, potentially offer enhanced heat transfer performance. For an extensive review about heat transfer of nanofluids, interested readers are referred to Das et al. [17]. Several studies have analyzed natural convection of nanofluids [18–20] where it has been observed that the nanoparticle volume fraction can affect the fluid flow and heat transfer characteristics. Furthermore, a recent study has considered the analysis of mixed convection of nanofluids [21] where it has been observed that the nanoparticle volume fraction can affect the fluid flow and heat transfer characteristics. However, to the best of the author's knowledge, the natural convection of nanofluids in enclosures with localized heating from the bottom wall and symmetrical cooling from the vertical sidewalls is yet to be analyzed in detail in the existing literature. Therefore, the current study addressed this gap in the existing literature by examining numerical simulations of natural convection of water-based nanofluids in enclosures with localized heating from the bottom wall and symmetrical cooling from the vertical sidewalls for different dimensionless heat source lengths ℓ/L ranging from 0.2 to 0.8, nanoparticle volume fractions φ ($0.00 \leq \varphi \leq 0.05$), and for different Rayleigh number Ra. The main objectives of the current study are, as follows:

1. To demonstrate the influences of ℓ/L, φ and Ra on the natural convection of water-based nanofluids in a square enclosure with partial heating from the bottom wall and symmetrical cooling from vertical sides.

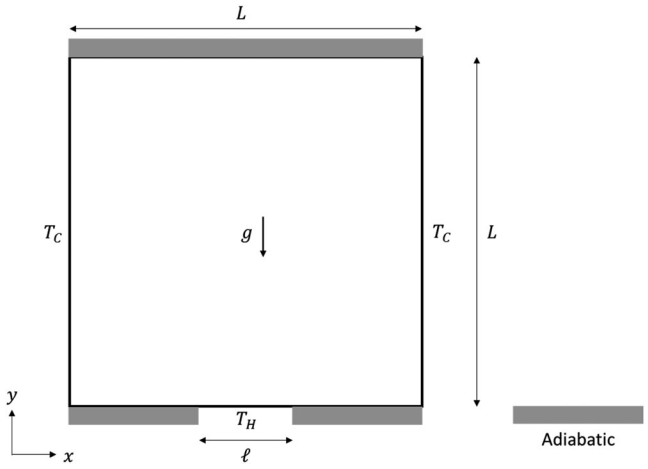

Figure 1. Schematic of considered configuration.

2. To provide physical explanations for the above effects and propose correlations for the mean Nusselt number $\overline{Nu}$ using the computational simulation data.

The remainder of the paper will be structured in the following manner. The mathematical background and numerical implementation will be presented in the next section. Subsequently, the results of the study will be presented along with the corresponding discussion. Finally, conclusions will be drawn, and the main findings will be summarized.

Mathematical background and numerical implementation

The schematic of the configuration considered in the current analysis is provided in Figure 1. The heated part of the bottom wall is considered to be at a temperature T_H, and the two vertical side walls are considered to be at a temperature T_C. It should be noted that $T_H > T_C$ is assumed. The remainder of the bottom wall and the top wall are considered to be adiabatic in nature. The no-slip condition is applied to all of the walls. In the current study, the flow is assumed to be laminar, incompressible, steady, and two-dimensional (i.e., the physical flow domain is assumed to be an infinitely long channel and, therefore, the third dimension is considered to not affect the flow and thermal fields). The non-dimensional conservation equations for mass, momentum, and energy in the cartesian coordinate system take the following form for steady-state, incompressible, two-dimensional flows, as considered in the current study:

$$\frac{\partial u_i^+}{\partial x_i^+} = 0 \tag{1a}$$

$$u_j^+ \frac{\partial u_i^+}{\partial x_j^+} = -\frac{\partial p^+}{\partial x_i^+} + \delta_{i2} Ra_{nf} Pr_{nf} + \frac{\partial \tau_{ij}^+}{\partial x_j^+} \tag{1b}$$

$$u_j^+ \frac{\partial \theta}{\partial x_j^+} = \frac{\partial^2 \theta}{\partial x_i^+ \partial x_j^+} \tag{1c}$$

where $x_i^+ = x_i/L$, $u_i^+ = u_i/U_{ref}$, $p^+ = p/\left(\rho U_{ref}^2\right)$, $\tau_{ij}^+ = \tau_{ij}/(\rho \alpha U_{ref})$, $\theta = (T - T_C)/(T_H - T_C)$ and $U_{ref} = \alpha_{nf}/L$ where $\alpha_{nf} = k_{eff}/[\rho_{nf}(c_p)_{nf}]$ is the effective thermal diffusivity of the nanofluid and L is the reference length scale. In Equation (1b), Ra_{nf} is the effective Rayleigh number of the nanofluid and Pr_{nf} is the effective Prandtl number of the nanofluid, which are defined as follows:

$$\begin{aligned} Ra_{nf} &= \frac{\rho_{nf}^2 g \beta_{nf} (c_p)_{nf} \Delta T L^3}{\mu_{eff} k_{eff}} \\ &= \left(\frac{\rho_{nf}}{\rho}\right)^2 \left(\frac{\beta_{nf}}{\beta}\right) \frac{(c_p)_{nf}}{c_p} \left(\frac{\mu}{\mu_{eff}}\right) \left(\frac{k}{k_{eff}}\right) \frac{g \beta \Delta T L^3}{\nu \alpha} \\ &= \left(\frac{\rho_{nf}}{\rho}\right)^2 \left(\frac{\beta_{nf}}{\beta}\right) \frac{(c_p)_{nf}}{c_p} \left(\frac{\mu}{\mu_{eff}}\right) \left(\frac{k}{k_{eff}}\right) Ra \end{aligned} \tag{2}$$

$$\begin{aligned} Pr_{nf} &= \frac{(c_p)_{nf} \mu_{eff}}{k_{eff}} = \frac{(c_p)_{nf}}{c_p} \left(\frac{\mu_{eff}}{\mu}\right) \left(\frac{k}{k_{eff}}\right) \frac{c_p \mu}{k} \\ &= \frac{(c_p)_{nf}}{c_p} \left(\frac{\mu_{eff}}{\mu}\right) \left(\frac{k}{k_{eff}}\right) Pr \end{aligned} \tag{3}$$

For the current study, it is assumed that the base-fluid (i.e., water) and nanoparticles (i.e., Al_2O_3) are in

thermal equilibrium, and that the thermophysical properties of the nanofluid are constant. The effective density (i.e., ρ_{nf}), specific heat (i.e., $(c_p)_{nf}$) and thermal expansion coefficient (i.e., β_{nf}) of a fluid containing suspended particles (i.e., a nanofluid) at a reference temperature (i.e., T_{ref}) are evaluated in the following manner [18, 21–23]:

$$\lambda_{nf} = (1-\varphi)\lambda_f + \varphi\lambda_s \tag{4}$$

where the subscripts "f" and "s" represent properties of base fluid and nanoparticles, and λ and φ are the property and the volume fraction of the nanoparticles, respectively. The effective viscosity of the nanofluid (i.e., μ_{eff}), which represents the viscosity of the base fluid (having a viscosity of μ_f) containing a dilute suspension of small rigid spherical particles, is given by Brinkman [24] as:

$$\mu_{eff} = \frac{\mu_f}{(1-\varphi)^{2.5}} \tag{5}$$

The effective thermal conductivity of the nanofluid (i.e., k_{eff}) can be given as [25, 26]:

$$k_{eff} = \frac{(k_s + 2k_f) - 2\varphi(k_f - k_s)}{(k_s + 2k_f) + \varphi(k_f - k_s)} k_s \tag{6}$$

where k_f and k_s are the thermal conductivities of the base fluid and the nanoparticles, respectively. Alternatively, other expressions for the effective thermal conductivity k_{eff} for spherical particles based nanofluids can be considered [27, 28]. One of the alternatives for alumina based nanofluid is given by [28]:

$$k_{eff} = 1 + 64.7\varphi^{0.764}\left(\frac{d_f}{d_s}\right)^{0.369}\left(\frac{k_f}{k_s}\right)^{0.7476} Pr^{0.9955}\ Re_f^{1.2321} \tag{7}$$

where $Re_f = \rho u_{bm} d_s/\mu$ is the base fluid Reynolds number, and $d_f = 0.27nm$ and $d_s = 11nm$ are the molecular diameters of the base fluid (i.e., water) and nanoparticle, respectively, and u_{bm} is the Brownian motion velocity of nanoparticles based on Einstein's diffusion theory. In the current study, the expression for k_{eff} given in Equation (6) will be considered for the numerical simulations. However, sensitivities using alternative expressions for k_{eff} (e.g., Equation (7)) will be carried out to ensure that any significant effects of using different expressions for k_{eff} are accounted for.

Using Buckingham's pi theorem, it is possible to express the mean Nusselt number $\overline{Nu}$ in this configuration as $\overline{Nu} = f(Ra, Pr,\ \varphi,\ \ell/L)$ where the Rayleigh number Ra and Prandtl number Pr of the base fluid which are defined as:

$$Ra = \frac{g\beta\Delta T L^3}{\nu\alpha},\quad Pr = \frac{c_p\mu}{k} \tag{8}$$

For current investigation, the local Nusselt number Nu, based on the heated wall, can be defined as $Nu = h\ell/k$ where the heat transfer coefficient h can be written as:

$$h = \left| -k\frac{\partial T}{\partial x_2}\Big|_{wf} \times \frac{1}{(T_H - T_C)} \right| \tag{9}$$

where the subscript "wf" refers to the condition of the fluid in contact with the wall. The thermophysical properties of water, Al_2O_3 nanoparticles and Al_2O_3-water nanofluids (for the volume fractions considered) are presented in Table 1.

In the current study, the governing equations of mass, momentum and energy have been numerically solved in the context of the finite-volume methodology using the commercial software package Ansys Fluent [29]. A second-order central difference scheme was used for the discretization of the diffusive terms and a second-order upwind scheme is used for the convective terms. The PISO (Pressure-Implicit with Splitting Operators) algorithm [29], which is an extension of the well-known SIMPLE (Semi-Implicit Method for Pressure Linked Equations) algorithm [29], is used for coupling the pressure and velocity components. The convergence criteria were set to 10^{-6} for all the relative (scaled) residuals. The boundary conditions considered for the current analysis are provided in Table 2.

For the current analysis, a range of numerical parameters will be considered: $\ell/L = 0.2,\ 0.4,\ 0.6,\ 0.8$; $\varphi = 0.0,\ 0.01,\ 0.02,\ 0.03,\ 0.04,\ 0.05$; and $Ra = 10^3,\ 10^4,\ 10^5,\ 10^6$ (where the considered Ra is based upon the base fluid (i.e., water) properties.

Table 1. Thermophysical properties of the base fluid, nanoparticles, and nanofluids [20] (N.B. the thermal conductivity k for the nanofluids is based on Equation (6)).

Physical Properties	Base Fluid (Water)	Nano-particles Al_2O_3	Nanofluid ($\varphi = 0.01$)	Nanofluid ($\varphi = 0.02$)	Nanofluid ($\varphi = 0.03$)	Nanofluid ($\varphi = 0.04$)	Nanofluid ($\varphi = 0.05$)
$c_p\ J/(kg\cdot K)$	4179	765	4049.87	3927.80	3812.23	3702.61	3598.60
ρ kg $/m^3$	997	3880	1025.83	1054.66	1083.49	1113.32	1141.15
$k\ W/(m\cdot K)$	0.613	40	0.630	0.649	0.667	0.686	0.705
β 1/K	2.1×10^{-4}	8.5×10^{-6}	2.02×10^{-4}	1.95×10^{-4}	1.88×10^{-4}	1.82×10^{-4}	1.75×10^{-4}
$\mu\ kg/(m\cdot s)$	0.855×10^{-3}	–	0.876×10^{-3}	0.899×10^{-3}	0.922×10^{-3}	0.947×10^{-3}	0.971×10^{-3}

Table 2. Boundary conditions for the considered configuration.

Heated Bottom Wall Section	$u_1^+ = u_2^+ = 0,\ \theta = 1$ at $\frac{1-(\ell/L)}{2} < x_1^+ < \frac{1+(\ell/L)}{2}$ and $x_2^+ = 0$
Adiabatic Bottom Wall Sections	$u_1^+ = u_2^+ = 0,\ \partial\theta/\partial x_2^+ = 0$ at $0 < x_1^+ < \frac{1-(\ell/L)}{2}$ and $\frac{1+(\ell/L)}{2} < x_1^+ < 1$ and $x_2^+ = 0$
Top Wall	$u_1^+ = u_2^+ = 0,\ \partial\theta/\partial x_2^+ = 0$ at $0 < x_1^+ < 1$ and $x_2^+ = 0$
Left Wall	$u_1^+ = u_2^+ = 0,\ \theta = 0$ at $x_1^+ = 0$ and $0 < x_2^+ < 1$
Right Wall	$u_1^+ = u_2^+ = 0,\ \theta = 0$ at $x_1^+ = 1$ and $0 < x_2^+ < 1$

Table 3. The details of the meshes considered in the mesh independence analysis (N.B. * indicates the mesh used in the numerical simulations).

Mesh Name	M1	M2	M3	M4*	M5
Mesh Details	40×40	80×80	160×160	320×320	400×400
Bias in x_1 direction	N/A	N/A	N/A	N/A	N/A
Bias in x_2 direction	5 (toward bottom and top walls)	5 (toward bottom and top walls)	5 (toward bottom and top walls)	5 (toward bottom and top walls)	5 (toward bottom and top walls)

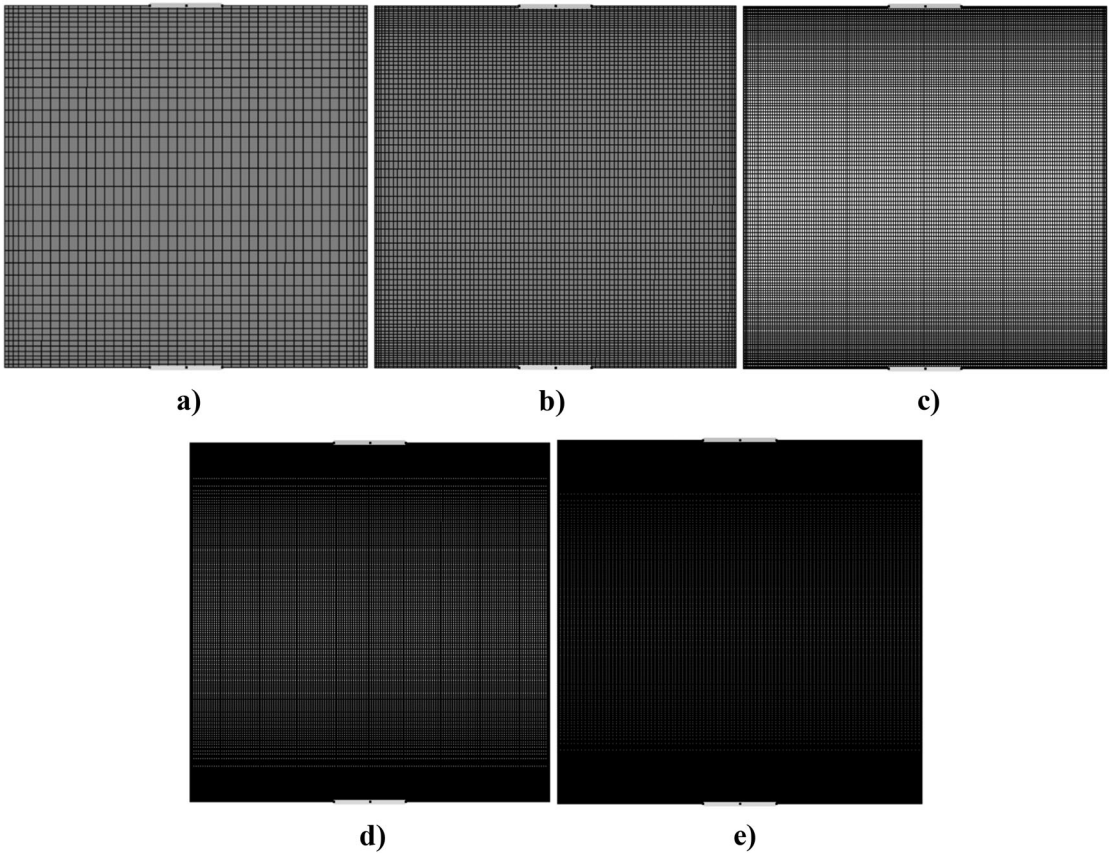

Figure 2. Considered meshes: a) M1, b) M2, c) M3, d) M4*, and e) M5. (N.B. *indicates the mesh used in the numerical simulations) shown for $\ell/L = 0.2$.

Accordingly, the computational mesh used in the current analysis is assessed to ensure mesh independence across the range of configurations and parameters considered. A total of 5 meshes (i.e., M1, M2, M3, M4 and M5) have been considered with the details of each mesh provided in Table 3, whereas Figure 2a–e shows the meshes used. It should be noted that no bias has been used in the x_1 direction whereas in the x_2 direction a bias factor of 5 is used toward the top and bottom walls. For meshes M1–M5, simulations were run for $\ell/L = 0.2$ and 0.8, for $\varphi = 0.0,\ 0.01$ and 0.05 where $Ra = 10^3$ and 10^6, resulting in 60 simulations considered for the mesh independence study. Figure 3a–f shows the variations in the mean Nusselt number $\overline{Nu}$ for $\ell/L = 0.2$ for $\varphi = 0.01 - 0.05$ and $Ra = 10^3 - 10^6$ in the case of meshes M1, M2, M3, M4, and M5. It is evident from Figure 3a–f that there is a small variation (i.e., within 0.1% for each configuration) in the value of the mean Nusselt number $\overline{Nu}$ from M4 to M5. To ensure the economic

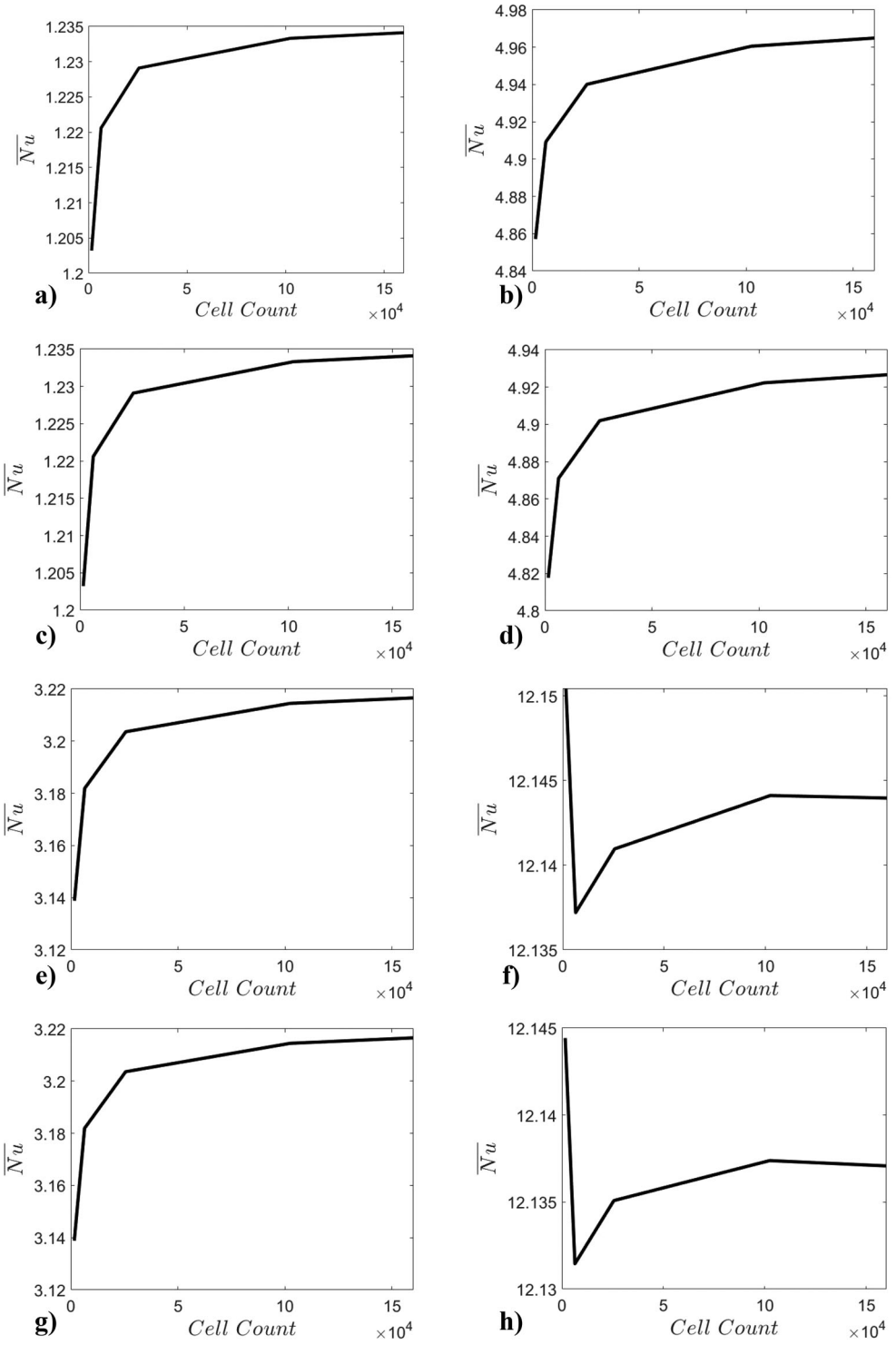

Figure 3. Variations in the mean Nusselt number $\overline{Nu}$ for the considered meshes M1, M2, M3, M4, and M5 shown for $\ell/L = 0.2$: a) $\varphi = 0.01$, $Ra = 10^3$, b) $\varphi = 0.01$, $Ra = 10^6$, c) $\varphi = 0.05$, $Ra = 10^3$, d) $\varphi = 0.05$, $Ra = 10^3$ and for $\ell/L = 0.8$: e) $\varphi = 0.01$, $Ra = 10^3$, f) $\varphi = 0.01$, $Ra = 10^6$, g) $\varphi = 0.05$, $Ra = 10^3$, h) $\varphi = 0.05$, $Ra = 10^6$.

feasibility of the study (over 200 simulations are considered) and appropriate accuracy, the mesh M4 has been used.

Further to the mesh independence analysis, the considered numerical set up, using mesh M4, has been benchmarked by comparing the results for the $\varphi = 0.00$ simulations with those of the seminal study by Aydin and Yang [11]. Figure 4 shows the variations of the mean Nusselt number $\overline{Nu}$ where $\varphi = 0.00$ simulations for (a) $\ell/L = 0.2$; (b) $\ell/L = 0.4$; (c) $\ell/L = 0.6$ and (d) $\ell/L = 0.8$ in the current study compared to Aydin and Yang [11]. It is evident from

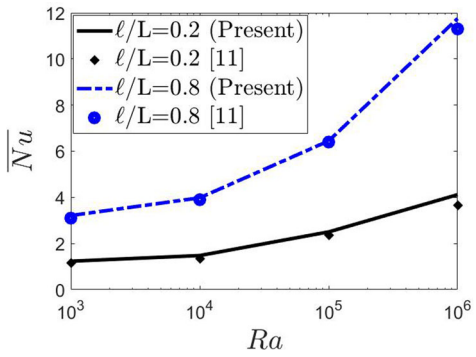

Figure 4. Variations on mean Nusselt number $\overline{Nu}$ across the heated surface for mesh M4 where $\varphi = 0.00$ for $\ell/L = 0.2$ and $\ell/L = 0.8$ for benchmarking with Aydin and Yang [11].

Figure 4 that there is an excellent agreement between the result of the current study and those of Aydin and Yang [11]. Accordingly, the chosen numerical set-up and mesh is deemed appropriate to adequately analyze the range of parameters considered in the current analysis.

Results and discussion

The laminar natural convection of water-based alumina nanofluids in a square enclosure with partial heating from the bottom and symmetrical cooling from the sides is considered in this section through the analysis of temperature fields, flow patterns and Nusselt number behavior for a range of values of Rayleigh number Ra, non-dimensional length of the isothermal heat source ℓ/L and nanoparticle volume fraction φ.

Behavior of streamlines and non-dimensional temperature θ

Figures 5 and 6 show the streamlines and the non-dimensional temperature θ across different Rayleigh numbers Ra (here based on the base fluid properties) in the case of $\varphi = 0.05$ for $\ell/L = 0.2$ and $\ell/L = 0.8$, respectively. The effects of varying the Rayleigh number Ra (i.e., $10^3 \leq Ra \leq 10^6$) and non-dimensional length of the isothermal heat source ℓ/L (i.e., $0.2 \leq \ell/L \leq 0.8$) can be seen from Figures 5 and 6, respectively. Given the symmetrical nature of the boundary conditions on the vertical walls, the streamlines, and contours of non-dimensional temperature θ are found to be symmetrical about the mid x_1-location of the enclosure. The distribution of the streamlines shows counter-rotating cells – one in the left half and one in the right half of the enclosure – which has been observed for all cases considered. The flows in the left and right half are found to be identical in magnitude but differing in the direction of rotation where the fluid ascends along the vertical line of symmetry, interacting with the adiabatic top surface before reaching the cold surface and descending. These observations are consistent with previous analyses [11] of laminar natural convection in a square enclosure with partial heating from the bottom and symmetrical cooling from the sides.

Figures 5 and 6 show that the distribution of the non-dimensional temperature θ changes significantly with the variation of Rayleigh number Ra. A Rayleigh number $Ra = 0$ corresponds to a pure conduction case where diffusion is the only heat transfer mechanism. For Rayleigh number $Ra = 10^3$ cases (see Figures 5e and 6e), the buoyancy forces are relatively weak, and conduction plays an important role in the transport of heat. As the Rayleigh number Ra increases, the buoyancy force strengthens and, therefore, it is found that the recirculation inside the square enclosure increases with convection playing a greater role in heat transfer which is demonstrated by the contours of the non-dimensional temperature θ becoming more distorted and the thickness of the thermal boundary layer on the vertical walls decreases with increasing Ra. These observations are consistent with previous analyses of laminar convection in a square enclosure with partial heating from the bottom and symmetrical cooling from the sides [11]. Importantly, it should be noted that the behavior of the streamlines and non-dimensional temperature θ contours are qualitatively similar for different φ values.

Behavior of local Nusselt number Nu

Further insight into the nature of the heat transfer can be obtained by considering the behavior of the local Nusselt number across the heated surface which is presented in Figure 7, which are representative of all cases considered. It is evident from Figure 7 that, due to the symmetrical nature of the non-dimensional temperature θ field, the local Nusselt number Nu is symmetrical about the mid x_1-location of the enclosure and is shown to increase with increasing Rayleigh number Ra. The higher the Rayleigh number Ra, the stronger the buoyancy forces and, therefore, the greater propensity for advection to play a role in the heat transfer relative to pure conduction and, accordingly, the local Nusselt number Nu increases. It should also be noted that the minimum local Nusselt number Nu is observed at the middle of the heated

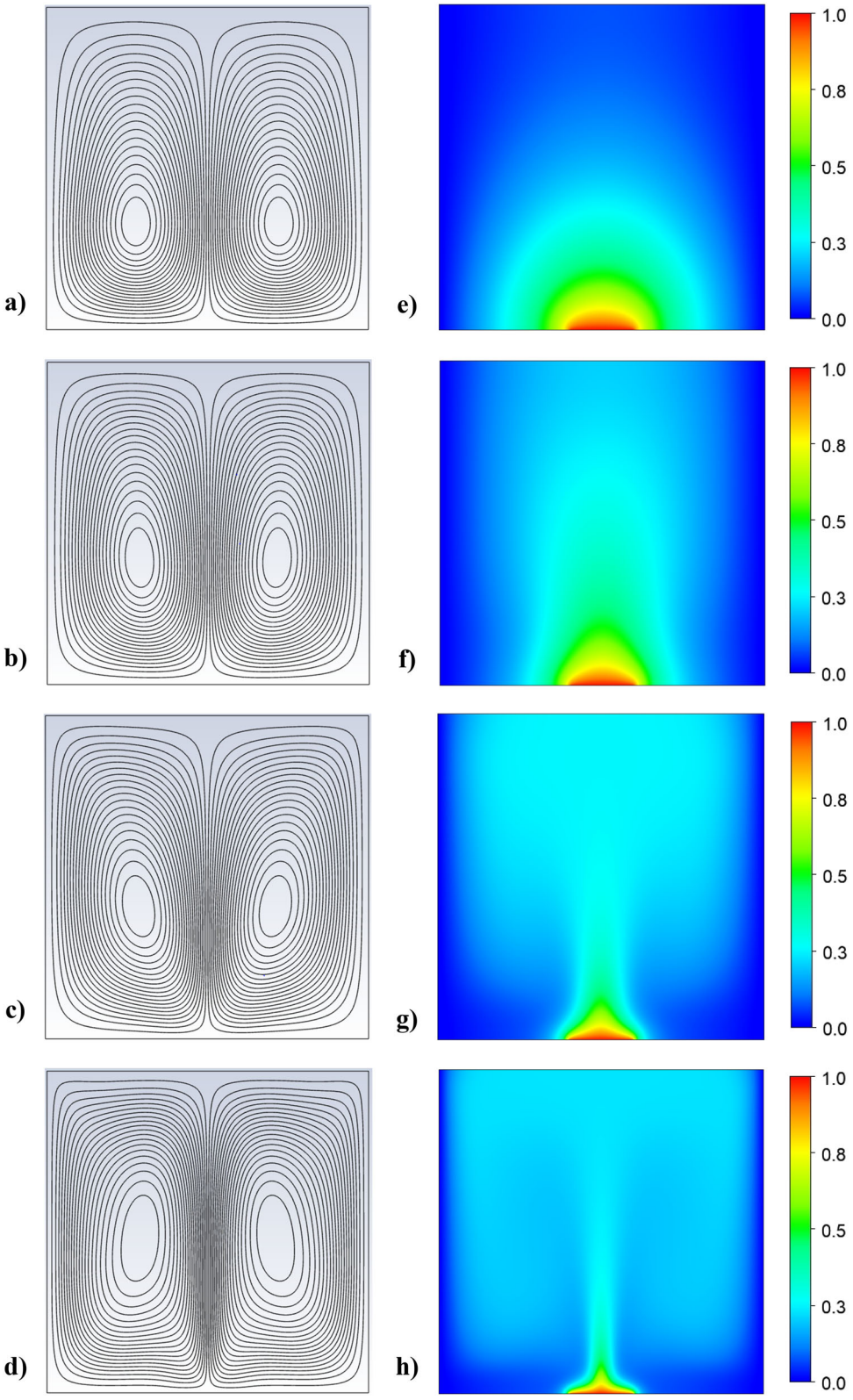

Figure 5. a)–d) Streamlines and e)–h) non-dimensional temperature θ contours for $Ra = 10^3$, 10^4, 10^5, and 10^6 (based on the base fluid properties) for $\varphi = 0.05$ and $\ell/L = 0.2$.

wall which is a consequence of the symmetrical boundary conditions applied in the vertical direction and the resulting circulating regions acting to reduce the effects of convection at this location. These observations are consistent with previous analyses of laminar convection in a square enclosure with partial heating from the bottom and symmetrical cooling from the sides [11].

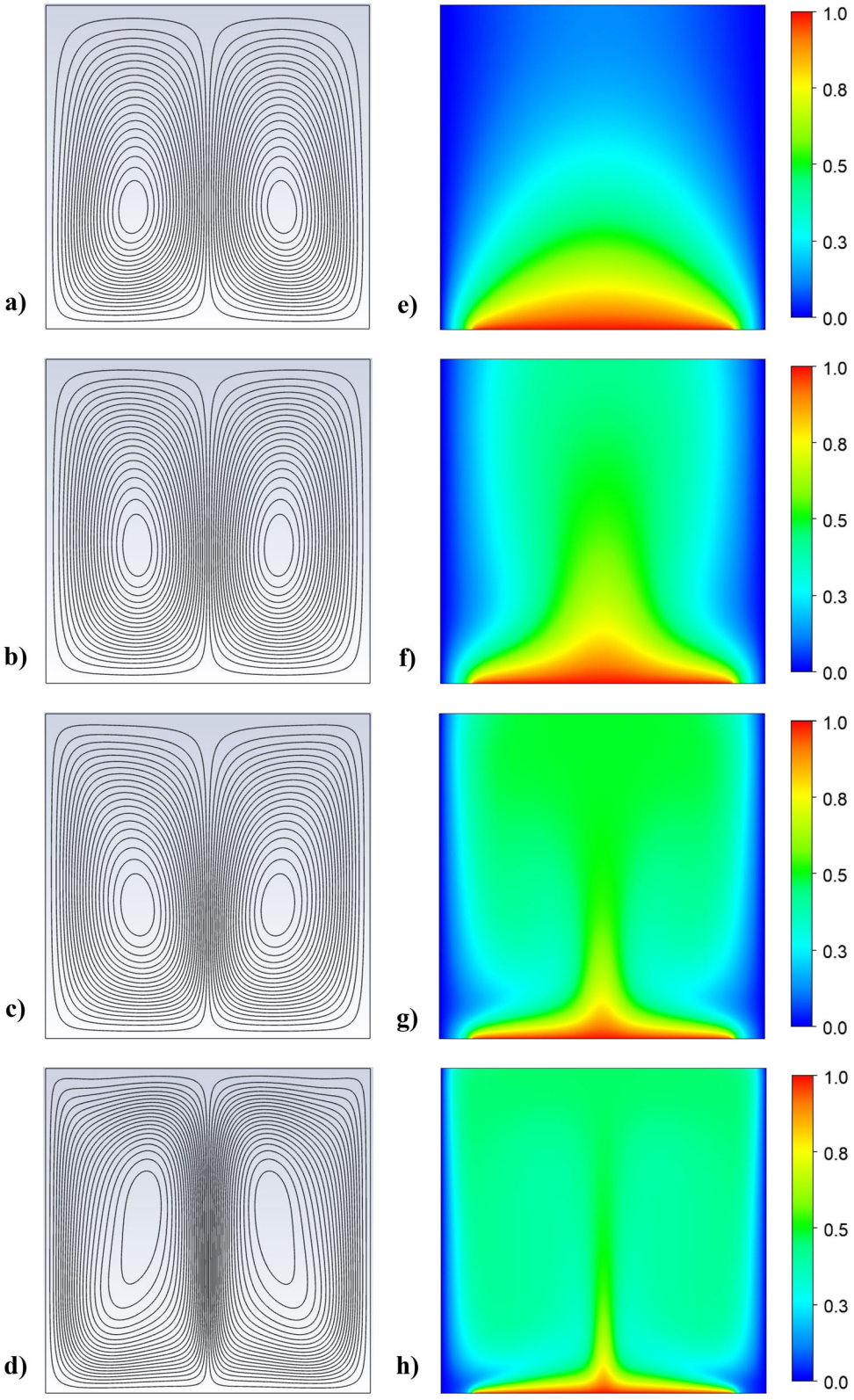

Figure 6. a)–d) Streamlines and e)–h) non-dimensional temperature θ contours for $Ra = 10^3$, 10^4, 10^5, and 10^6 (based on the base fluid properties) for $\varphi = 0.05$ and $\ell/L = 0.8$.

Behavior of non-dimensional vertical velocity U_2

Additional insights can be provided by considering the non-dimensional vertical velocity $U_2 = u_2.L/\alpha$ along the vertical line of symmetry which are shown in Figure 8. It is evident from Figure 8 that the non-dimensional vertical velocity U_2 increases with

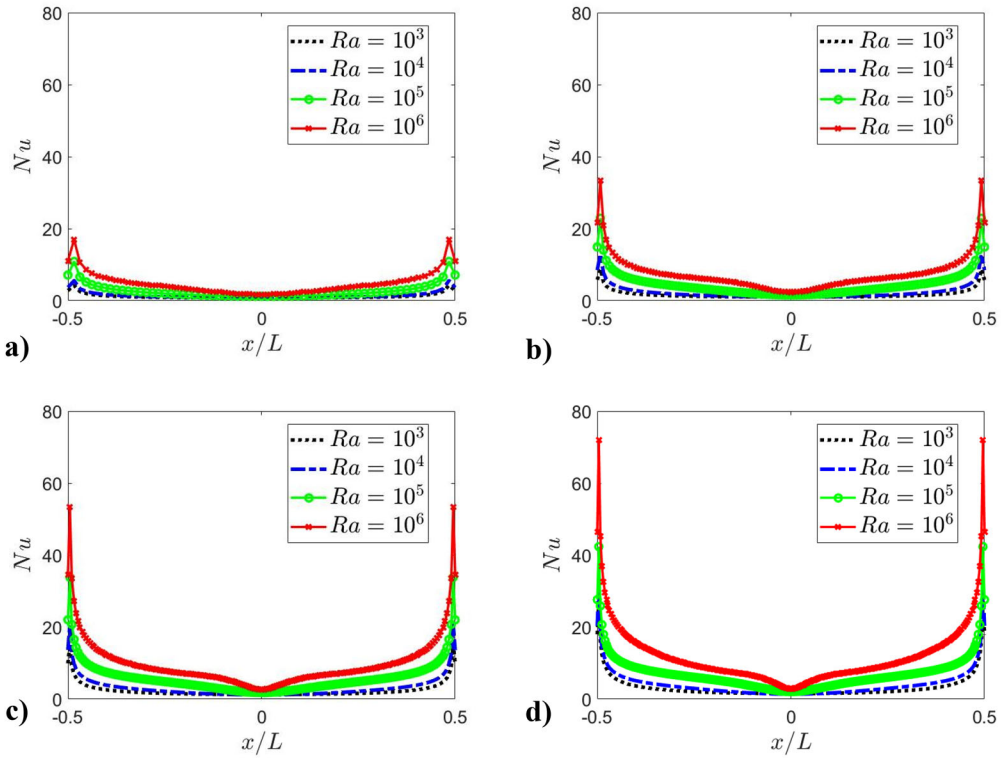

Figure 7. Variations of the local Nusselt number *Nu* across the hot surface for $Ra = 10^3$, 10^4, 10^5, and 10^6 (based on the base fluid properties) where $\varphi = 0.05$ for a) $\ell/L = 0.2$, b) $\ell/L = 0.4$, c) $\ell/L = 0.6$, and d) $\ell/L = 0.8$.

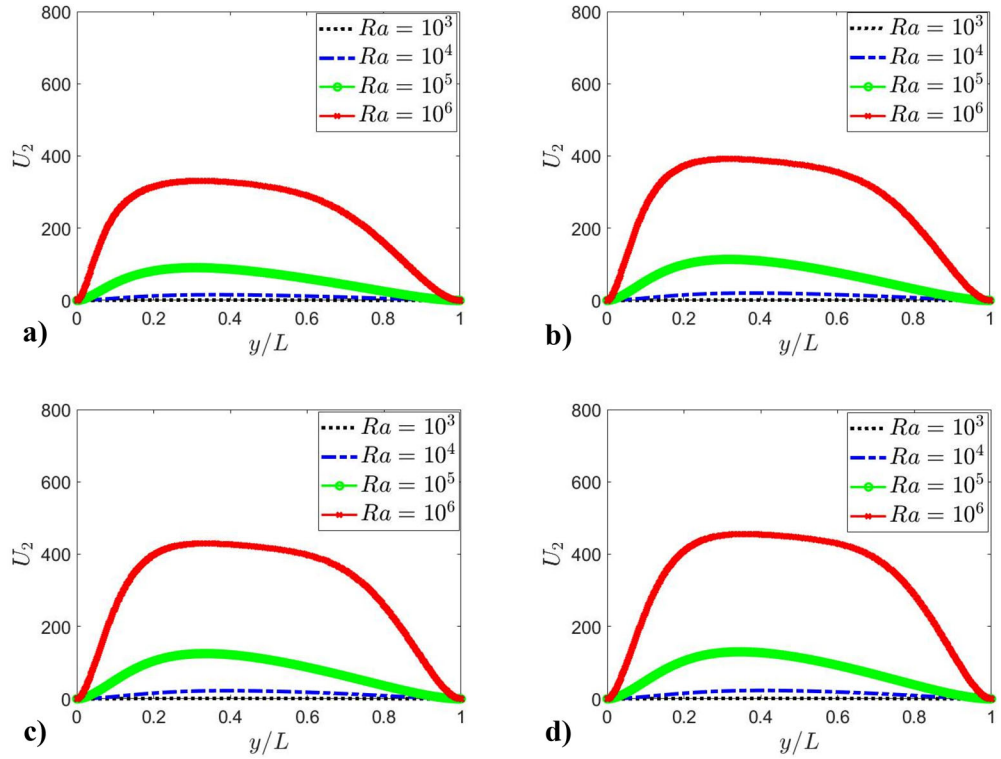

Figure 8. Variations of the non-dimensional vertical velocity U_2 along the vertical line of symmetry for $Ra = 10^3$, 10^4, 10^5, and 10^6 (based on the base fluid properties) where $\varphi = 0.05$ for a) $\ell/L = 0.2$, b) $\ell/L = 0.4$, c) $\ell/L = 0.6$, and d) $\ell/L = 0.8$.

increasing Rayleigh number *Ra* due to the strengthening of buoyancy forces. The variations of the mean Nusselt number $\overline{Nu}$ with Rayleigh number *Ra* are shown in Figure 9a–d for $\ell/L = 0.2$, 0.4, 0.6 and 0.8, respectively. It can be seen from Figure 9 that the mean Nusselt number $\overline{Nu}$ increases with increasing

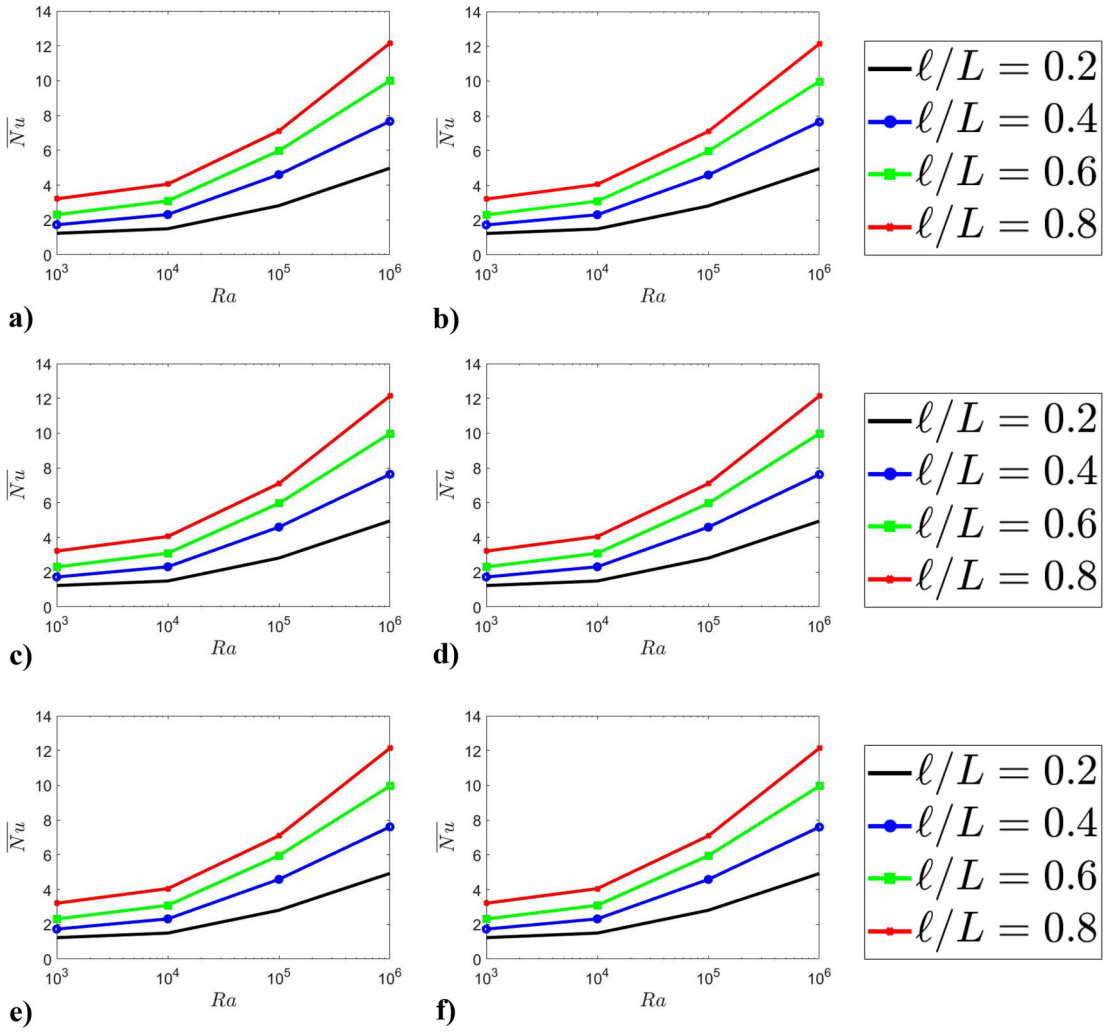

Figure 9. Variations of the mean Nusselt number $\overline{Nu}$ with Rayleigh number Ra (based on the base fluid properties) where $\ell/L = 0.2$, 0.4, 0.6, and 0.8 for a) $\varphi = 0.00$, b) $\varphi = 0.01$, c) $\varphi = 0.02$, d) $\varphi = 0.03$, e) $\varphi = 0.04$, and f) $\varphi = 0.05$.

Rayleigh number Ra due to the enhanced advective transport at higher Ra, which is consistent with previous analysis of laminar convection in a square enclosure with partial heating from the bottom and symmetrical cooling from the sides [11].

The effects of nanoparticle volume fraction φ

The variations of the mean Nusselt number $\overline{Nu}$ with nanoparticle volume fraction φ for $\ell/L = 0.2$, 0.4, 0.6, and 0.8 are shown in Figure 10a–d for $Ra = 10^3$, 10^4, 10^5, and 10^6, respectively, where the effective Rayleigh number is based on the base fluid properties. It should be noted that the variation of the nanoparticle volume fraction φ leads to changes in the thermophysical properties (see Table 1). Despite changes to the thermophysical properties due to the variation in φ, it is evident from Figure 10 that the mean Nusselt number $\overline{Nu}$ does not vary significantly with volume fraction φ for a given set of values of Rayleigh number Ra and normalized length of the heat source ℓ/L when considering values based upon the base fluid properties. Furthermore, the variations of the mean Nusselt number $\overline{Nu}$ with nanoparticle volume fraction φ for $\ell/L = 0.2$, 0.4, 0.6, and 0.8 are shown in Figure 11a–d for $Ra = 10^3$, 10^4, 10^5, and 10^6, respectively, where the effective Rayleigh number is based on the effective nanofluid properties. It should be noted that, in this instance, the mean Nusselt number at $Ra = 10^3$ does not vary significantly with the volume fraction φ. However, with increasing Ra (i.e., $Ra = 10^4$, 10^5 and 10^6), it can be seen that the mean Nusselt number decreases with increasing volume fraction φ across all values of ℓ/L. The above behaviors can be explained by considering the competition between buoyancy and viscous forces in the currently considered configuration.

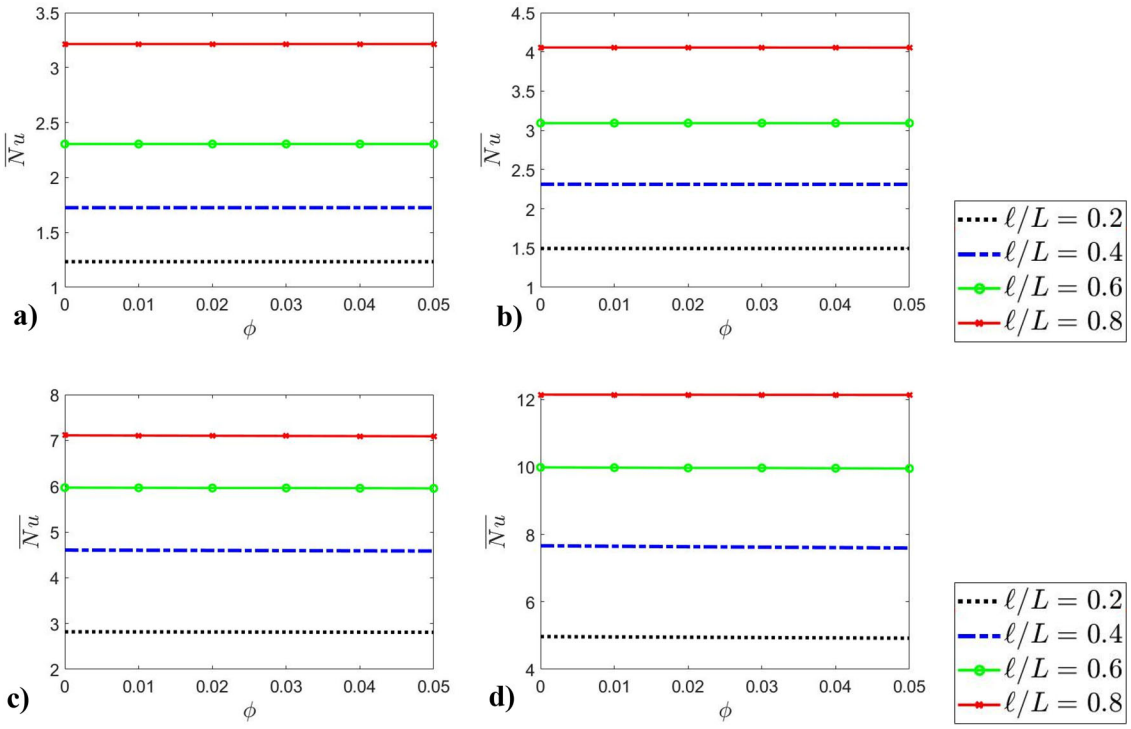

Figure 10. Variations of the mean Nusselt number $\overline{Nu}$ with volume fraction φ where Rayleigh number Ra is based on the base fluid properties where $\ell/L = 0.2,\ 0.4,\ 0.6,$ and 0.8 for a) $Ra = 10^3$, b) $Ra = 10^4$, c) $Ra = 10^5$, and d) $Ra = 10^6$.

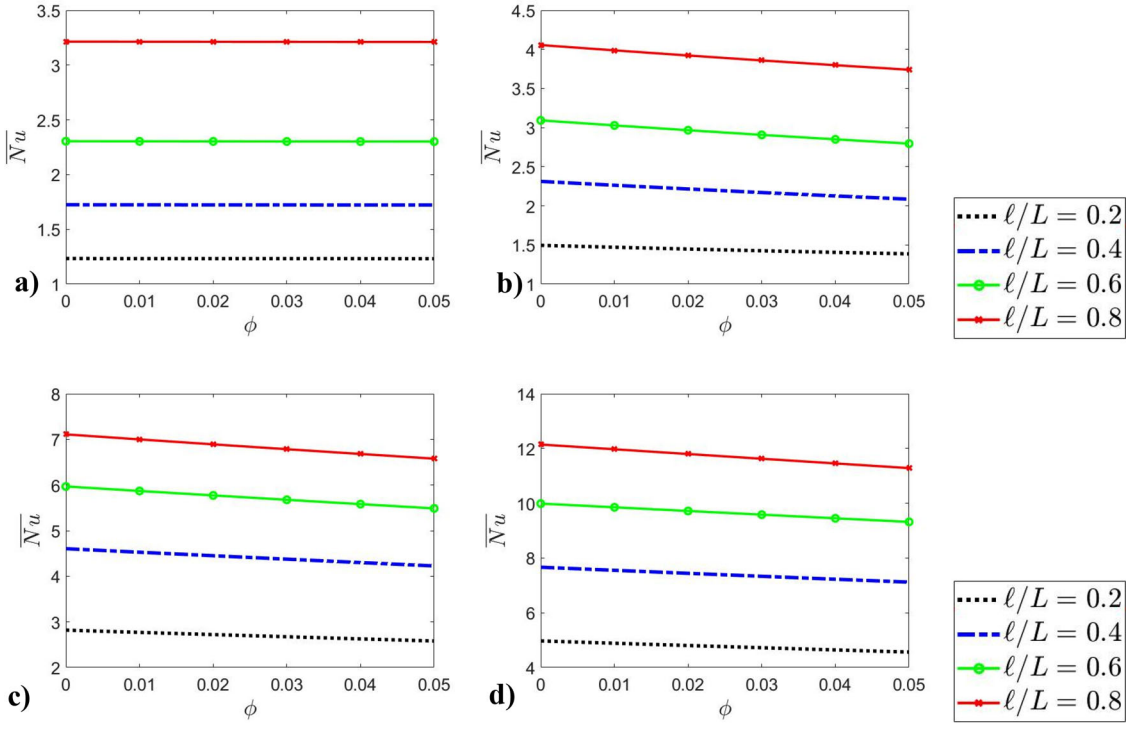

Figure 11. Variations of the mean Nusselt number $\overline{Nu}$ with volume fraction φ where the effective Rayleigh number Ra is based on the nanofluid properties where $\ell/L = 0.2,\ 0.4,\ 0.6,$ and 0.8 for a) $Ra_{nf} = 10^3$, b) $Ra_{nf} = 10^4$, c) $Ra_{nf} = 10^5$, and d) $Ra_{nf} = 10^6$.

Whilst the addition of nanoparticles increases the thermal conductivity of the fluid, the viscosity of the fluid also increases with increasing φ. The nanofluids have large effective Prandtl numbers (i.e., $Pr_{nf} \gg 1$). For $Pr_{nf} \gg 1$, the hydrodynamic boundary-layer thickness is thicker than the thermal

boundary layer thickness (i.e., $\delta \gg \delta_{th}$) and thus a considerable region of the hydrodynamic boundary layer remains unaffected by the presence of thermal boundary layer [30]. The order of magnitude analysis by Bejan [30] demonstrates that the balance between viscous and buoyancy forces governs the transport within the thermal boundary layer for $Pr_{nf} \gg 1$ (e.g., $Pr_{nf} \sim 10$), whereas the relative balances of inertial and viscous forces govern the transport behavior within the hydrodynamic boundary layer outside thermal boundary layer. Thus, a change in Prandtl number acts to modify the relative balance between viscous and inertial forces in natural convection, whereas the thermal transport within thermal boundary layer is marginally affected for $Pr_{nf} \gg 1$ (e.g., $Pr_{nf} \sim 10$) nanofluids. An increase in φ for a given value of Ra leads to an increase in thermal conductivity signifying the strengthening of thermal diffusive effects but also leads to a decrease in Ra_{nf} indicating weakening of thermal advection. These two effects counter each other and as a result $\overline{Nu}$ remains insensitive to the variation of φ when the values relating to the base fluid properties are considered. An increase in φ for a given value of Ra_{nf} acts to reduce the value of Pr_{nf} (e.g., 11% change between $\varphi = 0$ and 0.05), and it was demonstrated in past analyses (e.g., [31, 32]) that the heat and momentum transports within thermal and velocity boundary layers are altered in such a way (e.g., a drop in Pr_{nf} acts to thicken the thermal boundary layer with respect to the hydrodynamic boundary layer) that the advection effects weaken with a decrease in Prandtl number. This leads to a weakening to advective transport, which is reflected in the decrease in the mean Nusselt number with increasing volume fraction.

The effects of normalized length of the heat source ℓ/L

It is evident from Figure 8 that the mean Nusselt number $\overline{Nu}$ increases with increasing normalized length of the heat source ℓ/L for a given set of values of Rayleigh number Ra and volume fraction φ. This behavior originates due to the strengthening of advective transport with an increase in the normalized length of the heat source ℓ/L, irrespective of the values of Ra and φ, which can be confirmed by increased magnitudes of local Nusselt number Nu and U_2 for higher values of ℓ/L in Figures 7 and 8, respectively. Furthermore, a comparison between Figures 5 and 6 reveals that the isotherms become increasingly curved, and the thermal boundary layer becomes increasingly thin with increasing ℓ/L for a given value of Ra due to the strengthening of advective transport. This is reflected in the increasing trend of $\overline{Nu}$ with an increase in ℓ/L. These observations are consistent with previous analyses of both Newtonian [11] and non-Newtonian [33] fluids in this configuration.

The effect of thermal conductivity of the nanofluid k_{eff} model

It should be noted that a number of different models have been proposed for the effective thermal conductivity of the nanofluid k_{eff} as outlined earlier in this paper. In this section, a comparison of the results where the thermal conductivity k_{eff} is based upon Equations (6) and (7) is provided. In Figure 12 the variations of the mean Nusselt number $\overline{Nu}$ with Rayleigh number Ra for $\ell/L = 0.2$ are shown different values of volume fraction φ for k_{eff} approximations based on Equations (6) and (7). It is evident from Figure 12 that the qualitative and quantitative behavior of the mean Nusselt number $\overline{Nu}$ is not sensitive to the choice of the effective thermal conductivity k_{eff}.

Modeling of the mean Nusselt number $\overline{Nu}$

A correlation for the mean Nusselt number $\overline{Nu}$ can be proposed based upon scaling arguments. The wall heat flux q can be scaled as:

$$q \sim k_{eff} \frac{\Delta T}{\delta_{th}} \sim h \Delta T \tag{10}$$

Thus, the mean Nusselt number $\overline{Nu}$ can be scaled as:

$$\overline{Nu} \sim \frac{h\ell}{k} \sim \frac{\ell}{\delta_{th}} \sim \frac{\ell}{\delta} f_1(Ra, Pr, \varphi, \ell/L) \tag{11}$$

where f_1 is a function of Ra, Pr, φ and ℓ/L which accounts for the ratio of hydrodynamic to thermal boundary layer thicknesses (i.e., $\delta/\delta_{th} \sim f_1(Ra, Pr, \varphi, \ell/L)$). The order of magnitude analysis of momentum transport in the vertical direction yields [9, 33]:

$$\rho_{nf} \frac{V^2}{L} \sim \rho_{nf} g \beta_{nf} \Delta T \tag{12}$$

where V is the characteristic velocity scale in the vertical direction. Equation (12) yields $V \sim \sqrt{g \beta_{nf} \Delta T L}$, which upon using the equality of the order of magnitude estimates of inertial and viscous term yields an

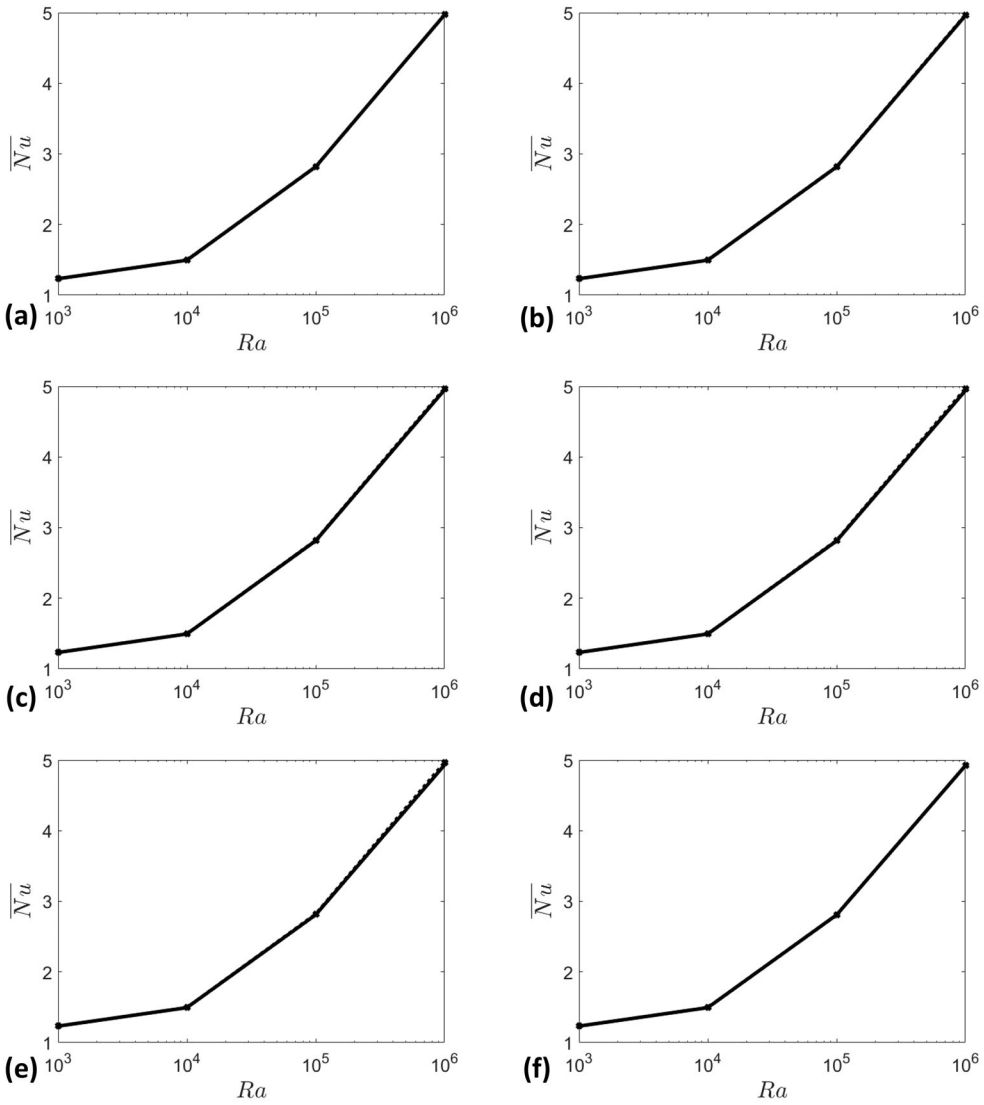

Figure 12. Variations of the mean Nusselt number $\overline{Nu}$ with Rayleigh number Ra (based on the base fluid properties) along the heated surface for the effective thermal conductivity k_{eff} is based on Eq. 6 (▬▬) and Eq. 7 (■ ■ ■■ ■) where $\ell/L = 0.2$ for a) $\varphi = 0.00$, b) $\varphi = 0.01$, c) $\varphi = 0.02$, d) $\varphi = 0.03$, e) $\varphi = 0.04$, and f) $\varphi = 0.05$.

estimate of the hydrodynamic boundary layer thickness [9, 33]:

$$\rho_{nf}\frac{V^2}{L} \sim \rho_{nf} g \beta_{nf} \Delta T \sim \mu_{nf}\frac{V}{\delta^2} \tag{13}$$

Equation (13) provides:

$$\begin{aligned} \delta &\sim \frac{L}{\left[Ra_{nf}\ \ Pr_{nf}\ ^{-1}\right]^{1/4}} \text{ and} \\ \delta_{th} &\sim \frac{L}{\left[Ra_{nf}\ \ Pr_{nf}\ ^{-1}\right]^{1/4} f_1(Ra, Pr, \varphi, \ell/L}) \end{aligned} \tag{14}$$

Using Equation (14) in Equation (11) provides the following scaling estimate of the mean Nusselt number $\overline{Nu}$ in the following manner:

$$\overline{Nu} \sim (\ell/L)\left[Ra_{nf}\ \ Pr_{nf}\ ^{-1}\right]^{\frac{1}{4}} f_1(Ra, Pr, \varphi, \ell/L) \tag{15}$$

Guided by Equation (15) a correlation for the mean Nusselt number $\overline{Nu}$ is proposed here in the following manner:

$$\overline{Nu} = \max\{1.0(\ell/L)^{c^*}\left[Ra_{nf}\ \ Pr_{nf}\ ^{-1}\right]^{1/4}\left(\frac{\rho_{nf}}{\rho}\right)^{-1/2} \left(\frac{\beta_{nf}}{\beta}\right)^{-\frac{1}{4}}\left(\frac{\mu}{\mu_{eff}}\right)^{-1/2}, 1.0\} \text{ with } c^* = 0.777 \tag{16}$$

It is evident from Figure 13a–c that the expression presented in Equation (16) adequately captures the qualitative and quantitative behavior (i.e., $R^2 = 0.94$)

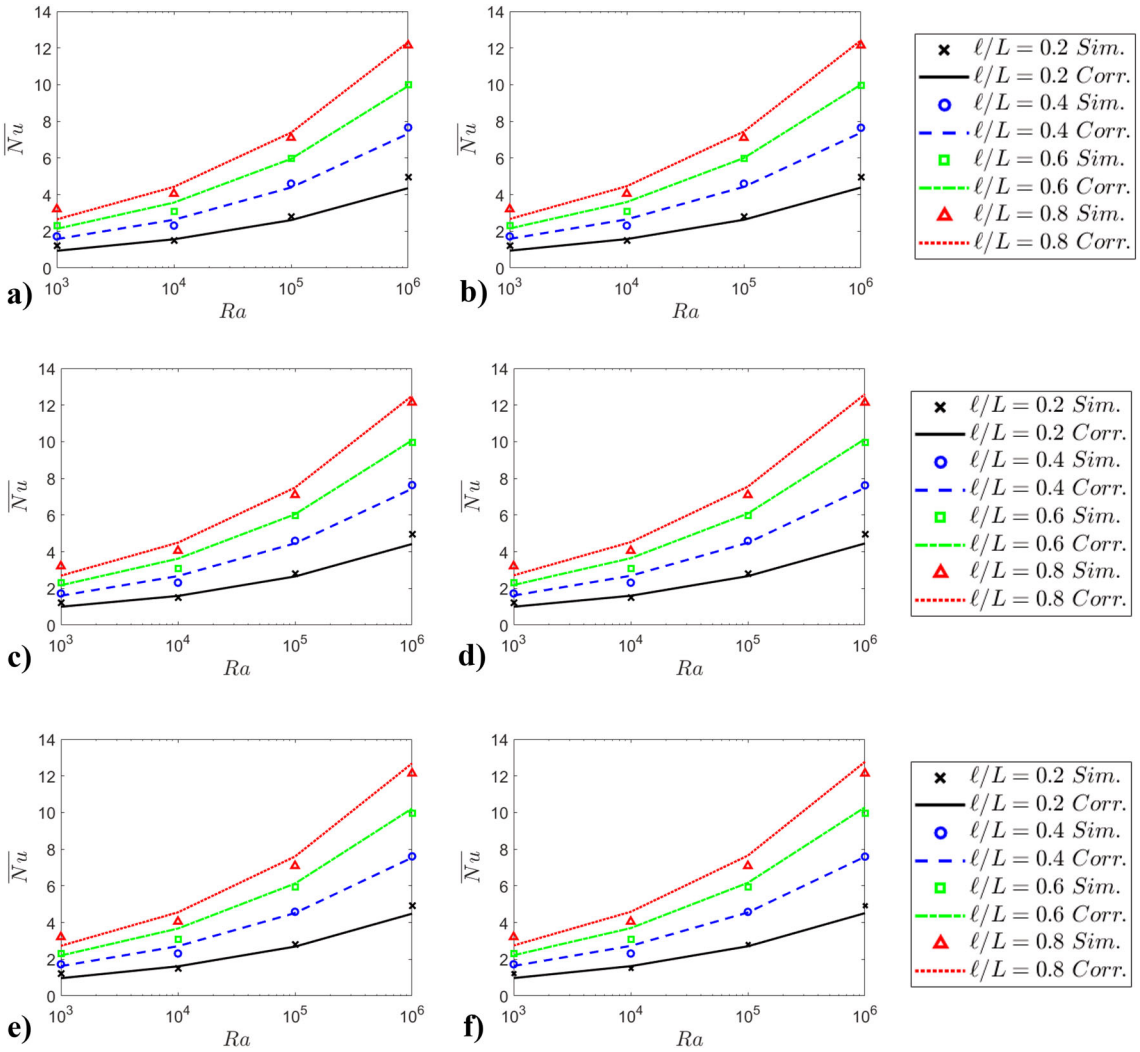

Figure 13. Variations of the mean Nusselt number $\overline{Nu}$ with Rayleigh number Ra (based on the base fluid properties) along with the values given by Equation (16) where $\ell/L = 0.2,\ 0.4,\ 0.6,$ and 0.8 for a) $\varphi = 0.00$, b) $\varphi = 0.01$, c) $\varphi = 0.02$, d) $\varphi = 0.03$, e) $\varphi = 0.04$, and f) $\varphi = 0.05$.

of the mean Nusselt number $\overline{Nu}$ across the range of Rayleigh numbers Ra, normalized heated surface length ℓ/L and volume fraction φ considered in the current analysis.

Conclusions

Steady-state, laminar, natural convection of water-based alumina nanofluids in a square enclosure with partial heating from the bottom and symmetrical cooling from sides has been investigated based on numerical simulations. The partial heating is achieved by a centrally located heat source on the bottom wall for different values of normalized heat source length ℓ/L (i.e., $\ell/L = 0.2,\ 0.4,\ 0.6$ and 0.8), nominal Rayleigh number Ra based on base fluid properties (i.e., $Ra = 10^3,\ 10^4,\ 10^5$ and 10^6) and alumina volume fraction φ (i.e., $\varphi = 0.0,\ 0.01,\ 0.02,\ 0.03,\ 0.04$ and 0.05). The effects of Rayleigh number Ra, normalized heat source length ℓ/L and nanoparticle volume fraction φ on the nature of the heat transfer in the currently considered configuration have been investigated in detail. It has been found that the nominal Rayleigh number Ra, for a given value of ℓ/L and φ, leads to an increase in Nusselt number Nu due to the strengthening of thermal advective transport. This has been verified from the increase in the magnitude of the vertical velocity component with increasing Rayleigh number Ra due to the strengthening of buoyancy forces. It has also been found that, for a given value of Ra and ℓ/L, the Nusselt number Nu is found to not vary significantly with increasing φ as the strengthening of viscous effects with increasing φ for the water-based alumina nanofluids counteracts the effects of enhanced thermal diffusion in nanofluids. However, for a given value of Ra and ℓ/L,

where the effective Rayleigh number is based on the nanofluid properties, the Nusselt number Nu is found to decrease with increasing φ. For a given value of Ra and φ, the Nusselt number is found to increase with increasing normalized length of the heat source ℓ/L which is due to the augmentation of the advective transport effects with an increase in ℓ/L. These observations are consistent with previous analyses of Newtonian and non-Newtonian fluids [11, 33]. It has been demonstrated that the choice of model for effective thermal conductivity k_{eff} has no significant influence on the mean Nusselt number. Finally, a scaling analysis has been utilized to propose a correlation for the mean Nusselt number $\overline{Nu}$ which has been demonstrated to adequately capture the qualitative and quantitative behavior obtained from the simulations across the ranges of Rayleigh number Ra, normalized length of the heat source ℓ/L and nanoparticle volume fraction φ considered in the current study.

Disclosure statement

No potential conflict of interest was reported by the authors.

Notes on contributors

Sean Malkeson is Program Leader in Mechanical Engineering in the School of Engineering at Liverpool John Moores University. He obtained his PhD from the University of Liverpool before working there as a lecturer. Subsequently, he obtained industrial experience working as a Consultant Engineer being involved in gas dispersion analyses, fire detection studies, fire modeling, heating, ventilation and air conditioning studies, and conjugate heat transfer problems on onshore and offshore installations as well as the assessment of the operational envelope of helicopter landings on oil platforms. His research interests include direct numerical simulations of turbulent combustion as well as the development of models for turbulent combustion in the context of Reynolds Averaged Navier Stokes simulations. He also has interests in the analysis of turbulent mixing and heat transfer in non-Newtonian fluids.

Nilanjan Chakraborty is a Professor of Fluid Dynamics at the School of Engineering of Newcastle University. Previously he was a senior lecturer at the School of Engineering of the University of Liverpool. He gained industrial experience as a Mechanical Engineer in General Electric, India before getting the prestigious Gates Cambridge Scholarship for pursuing a PhD at Cambridge University. His research interests include direct numerical simulations of turbulent combustion, combustion modeling in the context of Reynolds Averaged Navier Stokes and large eddy simulations, melting/solidification related heat transfer problems in classical manufacturing (e.g., casting, welding) and laser aided manufacturing applications (e.g., laser surface alloying) and natural convection of complex non-Newtonian fluids. In 2005, he and his coauthors were awarded the Gaydon Prize for the most significant UK contribution to the 30th International Symposium on Combustion. He was also awarded the Hinshelwood Prize for 2007 by the British Section of the Combustion Institute for his contribution to combustion science as a young member. In 2009, the Combustion Institute judged a paper coauthored by him to be the most significant paper presented in the droplet combustion colloquium of the 32nd International Combustion Symposium.

ORCID

Nilanjan Chakraborty http://orcid.org/0000-0003-1690-2036

References

[1] T. Fusegi, J. M. Hyun, K. Kumahara and B. Farouk, "A numerical study of three dimensional natural convection in a differentially heated cubical enclosure," *Int. J. Heat Mass Transf.*, vol. 34, no. 6, pp. 1543–1557, Jun. 1991. DOI: 10.1016/0017-9310(91)90295-P.

[2] G. De Vahl Davis, "Natural convection of air in a square cavity: a benchmark solution," *Int. J. Numer. Methods Fluids*, vol. 3, no. 3, pp. 249–264, May/Jun 1993. DOI: 10.1002/fld.1650030305.

[3] O. Turan, R. J. Poole and N. Chakraborty, "Influence of boundary conditions of laminar natural convection in rectangular enclosures with differentially heated side walls," *Int. J. Heat Fluid Flow*, vol. 33, no. 1, pp. 131–146, Feb. 2012. DOI: 10.1016/j.ijheatfluidflow.2011.10.009.

[4] G. B. Kim, J. M. Hyun and H. S. Kwak, "Transient buoyant convection of a power law non-Newtonian fluid in an enclosure," *Int. J. Heat Mass Transf.*, vol. 46, no. 19, pp. 3605–3617, Sep. 2003. DOI: 10.1016/S0017-9310(03)00149-2.

[5] M. Lamsaadi, M. Naïmi, and M. Hasnaoui, "Natural convection heat transfer in shallow horizontal rectangular enclosures uniformly heated from the side and filled with non-Newtonian power law fluids," *Energy Convers. Manage.*, vol. 47, no. 15–16, pp. 2535–2551, Sep. 2006. DOI: 10.1016/j.enconman.2005.10.028.

[6] S. Yigit and N. Chakraborty, "Influences of aspect ratio on natural convection of power law fluids in cylindrical annular space with differentially heated vertical walls," *Therm. Sci. Eng. Prog.*, vol. 2, pp. 151–164, Jun. 2017. DOI: 10.1016/j.tsep.2017.05.008.

[7] E. Bodenschatz, W. Pesch, and G. Ahlers, "Recent developments in Rayleigh–Bénard convection,"

Annu. Rev. Fluid Mech., vol. 32, no. 1, pp. 709–778, 2000. Jan. DOI: 10.1146/annurev.fluid.32.1.709.

[8] N. Ouertatani, N. Ben Cheikh, B. Ben Beya, and T. Lili, "Numerical simulation of two-dimensional Rayleigh-Bénard convection in an enclosure," *C. R. Mecanique*, vol. 336, no. 5, pp. 464–470, May 2008. DOI: 10.1016/j.crme.2008.02.004.

[9] O. Turan, F. Fotso-Choupe, J. Lai, R. J. Poole, and N. Chakraborty, "Boundary condition effects on laminar natural convection of power-law fluids in a square enclosure heated from below differentially heated horizontal walls," *Ind. Eng. Chem. Res.*, vol. 53, no. 1, pp. 456–473, Jan. 2014. DOI: 10.1021/ie4023447.

[10] S. Yigit, R. J. Poole, and N. Chakraborty, "Aspect ratio effects on laminar Rayleigh-Bénard convection of power-law fluids in rectangular enclosures: a numerical investigation," *Int. J. Heat Mass Transf.*, vol. 91, pp. 1292–1307, Dec. 2015. DOI: 10.1016/j.ijheatmasstransfer.2015.08.032.

[11] O. Aydin and W.-J. Yang, "Natural convection in enclosures with localized heating from below and symmetrical cooling from sides," *Int. J. Numer. Methods Heat Fluid Flow*, vol. 10, no. 5, pp. 518–529, Aug. 2000. DOI: 10.1108/09615530010338196.

[12] T. Y. Chu and C. E. Hichox, "Thermal convection with large viscosity variation in an enclosure with localized heating," *ASME J. Heat Transf.*, vol. 112, no. 2, pp. 388–395, May 1990. DOI: 10.1115/1.2910389.

[13] M. Hasnaoui, E. Bilgen, and P. Vasseour, "Natural convection heat transfer in rectangular cavities partially heated from below," *J. Thermophys. Heat Transf.*, vol. 6, no. 2, pp. 255–264, Apr.–Jun. 1992. DOI: 10.2514/3.353.

[14] E. Ntibarufata, M. Hasnaoui, E. Bilgen, and P. Vasseur, "Natural convection in partitioned enclosures with localized heating," *Int. J. Num. Meth. Heat Fluid Flow*, vol. 3, no. 2, pp. 133–143, Feb. 1993. DOI: 10.1108/eb017521.

[15] G. Saha, S. Saha, M. Q. Islam, and M. A. R. Akhanda, "Natural convection in enclosure with discrete isothermal heating from below," *J. Nav. Archit. Mar. Eng.*, vol. 4, no. 1, pp. 1–13, Jun. 1970. DOI: 10.3329/jname.v4i1.912.

[16] M. A. Hassan, M. Pathak, and M. K. Khan, "Natural convection of viscoplastic fluids in a square enclosure," *ASME J. Heat Transf.*, vol. 135, no. 12, pp. 122501, Dec. 2013. DOI: 10.1115/1.4024896.

[17] S. K. Das, S. U. S. Choi, and H. E. Patel, "Heat transfer in nanofluids - a review," *Heat Transf. Eng.*, vol. 27, no. 10, pp. 3–19, 2006. DOI: 10.1080/01457630600904593.

[18] K. Khanafer, K. Vafai, and M. Lightstone, "Buoyancy-driven heat transfer enhancement in a two-dimensional enclosure utilizing nanofluids," *Int. J. Heat Mass Transf.*, vol. 46, no. 19, pp. 3639–3653, Sep. 2003. DOI: 10.1016/S0017-9310(03)00156-X.

[19] X. Meng and Y. Li, "Numerical study of natural convection in a horizontal cylinder filled with water-based alumina nanofluid," *Nanoscale Res. Lett.*, vol. 10, pp. 142, Mar. 2015. DOI: 10.1186/s11671-015-0847-x.

[20] M. Corcione, S. Grignaffini, A. Quintino, E. Ricci, and A. Vallati, "Buoyancy induced convection of alumina-water nanofluids in laterally heated vertical slender cavities," *Heat Transf. Eng.*, vol. 39, no. 13–14, pp. 1103–1116, 2018. DOI: 10.1080/01457632.2017.1363609.

[21] S. Yigit, P. Baruah, and N. Chakraborty, "Laminar mixed convection of water-based alumina nanofluid in a cylindrical enclosure with a rotating end wall: a numerical investigation," *Heat Transf. Eng.*, vol. 41, no. 5, pp. 393–406, 2020. DOI: 10.1080/01457632.2018.1557939.

[22] C.-L. Chen, S.-C. Chang, C.-K. Chen, and C.-K. Chang, "Lattice Boltzmann simulation for mixed convection of nanofluids in a square enclosure," *Appl. Math. Model.*, vol. 39, no. 8, pp. 2436–2451, Apr. 2015. DOI: 10.1016/j.apm.2014.10.049.

[23] M. Muthtamilselvan, P. Kandaswamy, and J. Lee, "Heat transfer enhancement of copper water nanofluids in a lid-driven enclosure," *Commun. Nonlinear Sci. Numer. Simul.*, vol. 15, no. 6, pp. 1501–1510, Jun. 2010. DOI: 10.1016/j.cnsns.2009.06.015.

[24] H. C. Brinkman, "The viscosity of concentrated suspensions and solutions," *J. Chem. Phys.*, vol. 20, no. 4, pp. 571–571, 1952. DOI: 10.1063/1.1700493.

[25] J. C. Maxwell, *A Treatise on Electricity and Magnetism*. Oxford, United Kingdom: Clarendon Press, 1873.

[26] R. L. Hamilton and O. K. Crosser, "Thermal conductivity of heterogeneous two-component systems," *Ind. Eng. Chem. Fundam.*, vol. 1, no. 3, pp. 187–191, Aug. 1962. DOI: 10.1021/i160003a005.

[27] Q. Z. Xue, "Model for thermal conductivity of carbon nanotube-based composites," *Physica B*, vol. 368, no. 1–4, pp. 302–307, Nov. 2005. DOI: 10.1016/j.physb.2005.07.024.

[28] C. H. Chon, K. D. Kihm, S. P. Lee, and S. U. S. Choi, "Empirical correlation finding the role of temperature and particle size for nanofluid (Al_2O_3) thermal conductivity enhancement," *Appl. Phys. Lett.*, vol. 87, no. 15, pp. 153107, Oct. 2005. DOI: 10.1063/1.2093936.

[29] Ansys., Fluent User's Guide, Canonsburg, PA, 2020.

[30] A. Bejan, *Convection Heat Transfer*. New York, NY, USA: Wiley, 1984, DOI: 10.1002/9781118671627.

[31] O. Turan, N. Chakraborty, and R. Poole, "Laminar natural convection of Bingham fluids in a square enclosure with differentially heated side walls," *J. Non-Newton. Fluid Mech.*, vol. 165, no. 15–16, pp. 901–913, Aug. 2010. DOI: 10.1016/j.jnnfm.2010.04.013.

[32] A. Koca, H. F. Oztap, and Y. Varol, "The effects of Prandtl number on natural convection in triangular enclosures with localized heating from below," *Int. Commun. Heat Mass Transf.*, vol. 34, no. 4, pp. 511–519, Apr. 2007. DOI: 10.1016/j.icheatmasstransfer.2007.01.006.

[33] S. Yigit, M. Battu, O. Turan, and N. Chakraborty, "Free convection of power-law fluids in enclosures with partially heating from bottom and symmetrical cooling from sides," *Int. J. Heat Mass Transf.*, vol. 145, pp. 118782, Dec. 2019. DOI: 10.1016/j.ijheatmasstransfer.2019.118782.